

Quantum Generative Adversarial Networks for Learning and Loading Random Distributions

Christa Zoufal,^{1,2,*} Aurélien Lucchi,² and Stefan Woerner¹

¹*IBM Research – Zurich*

²*ETH Zurich*

(Dated: December 15, 2024)

Quantum algorithms have the potential to outperform their classical counterparts in a variety of tasks. The realization of the advantage often requires the ability to load classical data efficiently into quantum states. However, the best known methods for loading generic data into an n -qubit state require $\mathcal{O}(2^n)$ gates. This scaling can easily predominate the complexity of a quantum algorithm and, thereby, impair potential quantum advantage.

Our work demonstrates that quantum Generative Adversarial Networks (qGANs) facilitate efficient loading of generic probability distributions – implicitly given by data samples – into quantum states. More specifically, the qGAN scheme employs the interplay of a quantum channel, a variational quantum circuit, and a classical neural network to learn the probability distribution underlying training data samples and load it into the quantum channel.

Effectively, the scheme results in a quantum channel that loads the learned distribution with $\mathcal{O}(\text{poly}(n))$ gates. This distribution loading method can, thus, enable the exploitation of quantum advantage induced by other quantum algorithms, such as Quantum Amplitude Estimation.

We implement the qGAN distribution learning and loading method with Qiskit and test it using a quantum simulation as well as actual quantum processors provided by the IBM Q Experience. Furthermore, we employ quantum simulation to demonstrate the use of the trained quantum channel in a quantum finance application.

I. INTRODUCTION

The realization of many promising quantum algorithms is impeded by the assumption that data can be efficiently loaded into a quantum state [1–4]. So far, this may only be achieved for particular but not for generic data structures. In fact, the complexity of data loading can easily dominate the overall complexity of an otherwise advantageous quantum algorithm [5].

A common assumption considering data loading in quantum algorithms is that access to the required data is provided by a Quantum Random Access Memory (QRAM) [6]. Besides the fact that no efficient implementation of QRAM is known up to now, the scheme only describes the addressing and not the loading of data. Moreover, QRAM is suitable for single use only as the no-cloning theorem [7] prohibits ideal duplication of the quantum memory.

This work presents a feasible learning and loading scheme for generic probability distributions based on a generative model. The scheme utilizes a hybrid quantum-classical implementation of a Generative Adversarial Network (GAN) [8, 9] to train a quantum channel such that it reflects a probability distribution implicitly given by data samples.

In classical machine learning, GANs have proven useful for generative modeling. These algorithms employ two competing neural networks – a generator and a discriminator – which are trained alternately. Replacing either

the generator, the discriminator, or both with quantum systems translates the framework to the quantum computing context [10].

The first theoretic discussion of quantum GANs (qGANs) was followed by demonstrations of qGAN implementations. Some focus on quantum state estimation [11], i.e., finding a quantum channel whose output is an estimate to a given quantum state [12–14]. Others exploit qGANs to generate classical data samples in accordance with the training data’s underlying distribution [15–17].

In contrast, our qGAN implementation learns and loads probability distributions into quantum states. More specifically, the aim of the qGAN is not to produce samples in accordance with given classical training data samples but to train the quantum generator to create a quantum state which represents the data’s underlying distribution. The resulting quantum channel, given by the quantum generator, enables efficient loading of a probability distribution into a quantum state and – in contrast to QRAM – can be duplicated and reused as often as needed. It needs to be emphasized that applying this qGAN scheme for data loading facilitates the exploitation of quantum advantage with algorithms such as Quantum Amplitude Estimation (QAE) [4] or the HHL algorithm [1].

The remainder of this paper is structured as follows. Sec. II explains classical GANs. Then, the qGAN-based distribution learning and loading scheme is introduced in Sec. III. In Sec. IV, we discuss the exploitation of qGANs to facilitate quantum advantage in financial derivative pricing: First, we discuss the training of the qGAN with data samples drawn from a log-normal distribution and present the results obtained with a quantum simulator

*Electronic address: ouf@zurich.ibm.com

and the IBM Q 20 Poughkeepsie superconducting quantum computer with 20 qubits both accessible via the IBM Q Experience [18]. Then, the resulting quantum channel is used in combination with QAE to price a European call option. Finally, Sec. V presents the conclusions and a discussion on open questions and additional possible applications of the presented scheme.

II. GENERATIVE ADVERSARIAL NETWORKS

In the context of generative modeling, GANs [8, 9] have achieved impressive results. They represent a class of algorithms that employ two neural networks - a generator and a discriminator - to solve a generative task, namely the creation of random samples of a distribution that is implicitly given by the training data. One of the main advantages of using GANs is that they rely on a zero-sum game formulation rather than a standard log-likelihood maximization, which has been observed to induce undesirable learning behavior [8].

Suppose a classical training dataset $X = \{x^0, \dots, x^{k-1}\}$ sampled from an unknown probability distribution p_{real} . Let G_θ and D_ϕ denote the generator and the discriminator networks, respectively. The corresponding network parameters are given by $\theta \in \mathbb{R}^{m_g}$ and $\phi \in \mathbb{R}^{m_d}$. The generator G_θ translates samples from a fixed prior distribution p_{prior} into samples which shall be indistinguishable from samples of the real distribution p_{real} . The discriminator, on the other hand, tries to distinguish between data from the training set and the generator. Fig. 1 illustrates the training process.

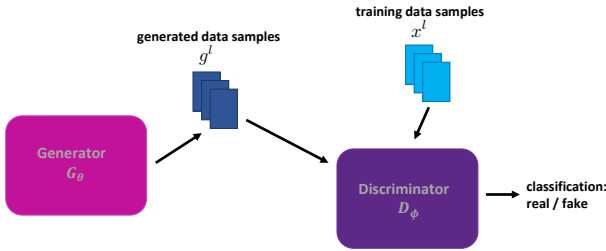


FIG. 1 Generative Adversarial Network: First, the generator creates data samples which shall be indistinguishable from the training data. Second, the discriminator tries to differentiate between the generated samples and the training samples. The generator and discriminator are trained alternately.

The optimization objective of classical GANs may be defined in various ways. In this work, we consider the non-saturating loss [19] which is also used in the code of the original GAN paper [8]. The generator's loss function

$$L_G(\phi, \theta) = -\mathbb{E}_{z \sim p_{\text{prior}}} [\log(D_\phi(G_\theta(z)))] \quad (1)$$

aims at maximizing the probability that the generator creates samples that are labeled as real data samples. On the other hand, the discriminator's loss function

$$L_D(\phi, \theta) = \mathbb{E}_{x \sim p_{\text{real}}} [\log D_\phi(x)] + \mathbb{E}_{z \sim p_{\text{prior}}} [\log(1 - D_\phi(G_\theta(z)))] \quad (2)$$

aims at maximizing the probability that the discriminator labels training data samples as training data samples and generated data samples as generated data samples.

In practice, the expected values are approximated by batches of size m

$$L_G(\phi, \theta) = -\frac{1}{m} \sum_{l=1}^m [\log(D_\phi(G_\theta(z^l)))] , \text{ and} \quad (3)$$

$$L_D(D_\phi, G_\theta) = \frac{1}{m} \sum_{l=1}^m [\log D_\phi(x^l) + \log(1 - D_\phi(G_\theta(z^l)))] , \quad (4)$$

for $x^l \in X$ and $z^l \sim p_{\text{prior}}$.

Training the GAN is equivalent to searching for a Nash-equilibrium of a two-player game:

$$\max_{\theta} L_G(\phi, \theta) \quad (5)$$

$$\max_{\phi} L_D(\phi, \theta) . \quad (6)$$

Typically, the optimization of Eq. (5) and Eq. (6) employs alternating update steps for the generator and the discriminator. These alternating steps lead to non-stationary objective functions, i.e., an update of the generator's (discriminator's) loss function also changes the parameters of the discriminator's (generator's) loss function. Gradient-based methods, such as ADAM [20] or AMSGRAD [21], are particularly well suited for solving such non-stationary objective functions [20].

III. QGAN DISTRIBUTION LEARNING

Our qGAN implementation uses a **quantum** generator and a **classical** discriminator to capture the probability distribution of **classical** training samples.

A quantum channel, i.e., the quantum generator, is trained to transform a given n -qubit input state $|\psi_{\text{in}}\rangle$ to an n -qubit output state

$$G_\theta |\psi_{\text{in}}\rangle = |g_\theta\rangle = \sum_{j=0}^{2^n-1} \sqrt{p_\theta^j} |j\rangle , \quad (7)$$

where p_θ^j describe the resulting occurrence probabilities of the basis states $|j\rangle$.

The aim of the qGAN training is to generate a state $|g_\theta\rangle$ whose p_θ^j describe a probability distribution that is

close to the distribution underlying the training data $X = \{x^0, \dots, x^{k-1}\}$. For simplicity, we now assume $X \subset \{0, \dots, 2^n - 1\}$ and, thus, the existence of a natural mapping between X and the states that can be represented by the generator. This assumption can be easily relaxed, for instance, by introducing an affine mapping between $\{0, \dots, 2^n - 1\}$ and an equidistant grid suitable for X . In this case, it might be necessary to map points in X to the closest grid point to allow for an efficient training. The number of qubits, n , determines the distribution loading scheme's resolution, i.e., the number of discrete values that can be represented.

During the training, this affine mapping can be applied after measuring the quantum state. But, when the resulting quantum channel is used as part of another quantum algorithm, it must be implemented with quantum gates. As it was discussed in [22], an affine map can be implemented in a gate-based quantum circuit with linearly many gates.

To train the qGAN, samples are drawn by measuring the output state $|g_\theta\rangle$ in the $Z^{\otimes n}$ -basis, where the set of possible measurement outcomes is $|j\rangle$, $j \in \{0, \dots, 2^n - 1\}$. Unlike in the classical case, the sampling does not require a stochastic input but is based on the inherent stochasticity of quantum measurements.

The scheme can be easily extended to d -dimensional distributions by choosing d qubit registers with n_i qubits each, for $i = 1, \dots, d$, and constructing a multi-dimensional grid equivalently to the 1-dimensional case, see Appendix A for an explicit example of a qGAN trained on multivariate data.

Next, we describe the constituents and the training of the quantum generator in more detail.

Choosing a suitable input state $|\psi_{\text{in}}\rangle$ close to the real distribution can speed up the training as well as help to avoid local optima and barren plateaus [23] in the quantum circuit training. To avoid that this preparation dominates the quantum generator's gate complexity, $|\psi_{\text{in}}\rangle$ must be loadable with $\mathcal{O}(\text{poly}(n))$ gates, which is, e.g., feasible with log-concave distributions [24].

The quantum generator is implemented by a variational form [25], i.e., a parametrized quantum circuit consisting of alternating layers of parametrized single-qubit rotations, here Pauli Y-rotations (R_Y) [3], and two-qubit gates, here controlled-Z gates (CZ) [3], called *entanglement block* U_{ent} , see Fig. 2(b). The circuit consists of a first layer of R_Y gates, and then k alternating repetitions of U_{ent} and further layers of R_Y gates. The parameter k is called the *depth* of the variational circuit, see Fig. 2(a). It follows that a variational circuit acting on n qubits uses in total $(k+1)n$ single-qubit gates and kn two-qubit gates.

Similarly to increasing the number of layers in deep neural networks [26], increasing the depth k enables the circuit to represent more complex structures.

Another possibility to increase the quantum generator's ability to represent complex correlations is adding ancilla qubits as this facilitates an isometric, instead of

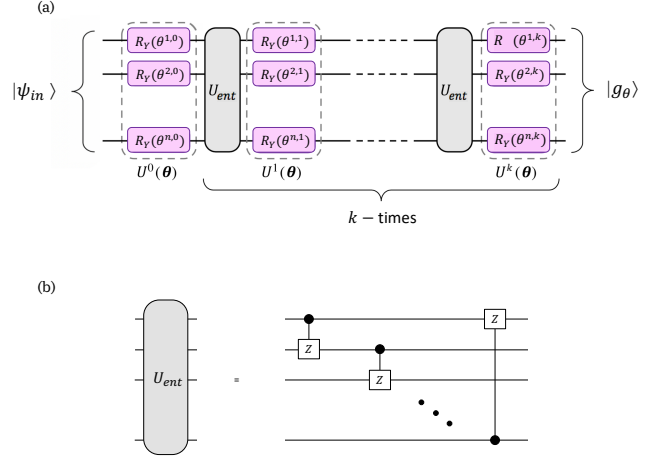


FIG. 2 The variational form, depicted in (a), with depth k acts on n qubits. It is composed of $k+1$ layers of single-qubit R_Y rotations and k entangling blocks U_{ent} . As illustrated in (b), each entangling block applies CZ gates from qubit i to qubit $(i+1) \bmod n$, $i \in \{0, \dots, n-1\}$ to create entanglement between the different qubits.

unitary, mapping [3], see Appendix B for more details.

The rationale behind choosing a variational form with R_Y and CZ gates, in contrast to other Pauli rotations and, e.g., CX gates, is that for $\theta^{i,j} = 0$ the variational form does not have any effect on the state amplitudes but only flips the phases. These phase flips do not perturb the effective probability distribution model which solely depends on the state amplitudes. Thus, if $|\psi_{\text{in}}\rangle$ is already close to the target state, then initializing all $\theta^{i,j}$ randomly but close to 0 potentially improves the training.

Given m data samples g^l from the quantum generator, and m randomly chosen training data samples x^l , where $l = 1, \dots, m$, the loss functions of the qGAN read

$$L_G(\phi, \theta) = -\frac{1}{m} \sum_{l=1}^m [\log(D_\phi(g^l))], \quad (8)$$

for the generator, and

$$L_D(\phi, \theta) = \frac{1}{m} \sum_{l=1}^m [\log D_\phi(x^l) + \log(1 - D_\phi(g^l))], \quad (9)$$

for the discriminator, respectively.

Equivalent to the classical case, see Eq. 5–6, the loss functions must be alternately maximized with respect to the generator's parameters θ and the discriminator's parameters ϕ . The optimization is preferably performed with gradient-based techniques to handle the non-stationary objectives and to speed up the convergence. Methods for the analytic computation of the quantum generator's gradients are discussed in Appendix C.

IV. APPLICATION IN QUANTUM FINANCE

We demonstrate the training and application of qGANs in the context of financial derivative pricing. More precisely, we employ qGANs to learn and load a model for the spot price of an asset underlying a European call option. Then, we use QAE [4] to estimate the fair price of the option [22].

A European call option holder is permitted, but not obliged, to buy an underlying asset for a given strike price K at a predefined future maturity date T . Given the asset's uncertain spot price at maturity S_T , the payoff reads $\max\{S_T - K, 0\}$. It follows that exercising the option is unreasonable if $S_T \leq K$. However, if $S_T > K$, exercising the option to buy the asset for price K and immediately selling it again for the market price S_T enables the exploitation of the payoff $S_T - K$. Now, the goal is to evaluate the expected payoff $\mathbb{E}[\max\{S_T - K, 0\}]$, whereby S_T is assumed to follow a given random distribution. This corresponds to the fair option price before discounting [27], which is neglected for simplicity.

According to the standard model for European option pricing, the Black-Scholes model [27], the spot price at maturity S_T is log-normally distributed. For our illustrative example, the Black-Scholes model is employed. Thus, we assume that p_{real} , which is typically unknown, is given by a log-normal distribution and generate the training data X by sampling from p_{real} .

The Black-Scholes model can be evaluated analytically. However, for more complex types of options or generic random distributions, classical evaluation of the expected payoff typically employs Monte Carlo simulation, which induces an estimation error behaving like $\mathcal{O}(1/\sqrt{N})$ for N samples of S_T . By using a QAE-based evaluation [22], we can improve the scaling quadratically to an error scaling as $\mathcal{O}(1/N)$. The implementation of the QAE-based evaluation of the expected payoff requires the random distribution underlying S_T to be loaded into a quantum state. We train a qGAN and use the resulting quantum channel to efficiently perform this loading step.

In the remainder of this section, we first illustrate the training of a qGAN using classical quantum simulation. Then, the results from a qGAN training run on actual quantum hardware are presented. Last, we show how the qGANs can facilitate QAE-based option pricing.

A. qGAN Training

Since the Black-Scholes model assumes that the spot price at maturity S_T for a European call option is log-normally distributed [27], we train the qGAN on samples from a truncated and discretized log-normal distribution.

The training data set X is constructed by sampling 10^4 times from a log-normal distribution with mean $\mu = 1$ and standard deviation $\sigma = 1$, discarding values outside the interval $[0, 7]$ and, then, rounding the values to integers, i.e., to the grid that can be represented by the

generator, namely $\{0, 1, \dots, 7\}$. We use a quantum generator that acts on $n = 3$ qubits, and, thus, enables the representation of $2^3 = 8$ values.

The quantum generator is implemented with Qiskit [28] which enables the circuit execution with quantum simulators as well as actual quantum hardware provided by the IBM Q Experience [18].

We choose to implement the quantum generator with a variational circuit with depth $k = 1$.

The generator's input state $|\psi_{\text{in}}\rangle$ is either prepared according to a discrete uniform distribution in $\{0, 1, \dots, 7\}$ or a truncated, discretized normal distribution with $\mu = 1$ and $\sigma = 1$ in $\{0, 1, \dots, 7\}$.

Loading a uniform distribution into a quantum state is simple as it only requires the application of one Hadamard gate per qubit [3]. Although the loading of a normal distribution involves more advanced techniques, the necessary $\mathcal{O}(\text{poly}(n))$ gates [24] will rarely predominate the quantum algorithm's overall gate complexity. Since the normal distribution is significantly closer to the target distribution, we expect the increased loading complexity to pay off with better performance.

The generator's parameters θ are initialized with random draws from a uniform distribution on the interval $[-\delta, +\delta]$. The following cases are considered:

1. Given a uniform $|\psi_{\text{in}}\rangle$, we set $\delta = 10^{-2}$ and, thus, start with $|g_\theta\rangle$ close to a uniform distribution.
2. Given a uniform $|\psi_{\text{in}}\rangle$, we set $\delta = \pi$ and, thus, start with a randomly chosen $|g_\theta\rangle$.
3. Given a normal $|\psi_{\text{in}}\rangle$, we set $\delta = 10^{-2}$ and, thus, start with $|g_\theta\rangle$ close to a normal distribution.

From now on, we refer to 1. as *uniform* initialization, to 2. as *random* initialization, and to 3. as *normal* initialization.

The discriminator, a classical neural network, is implemented with PyTorch [29]. The neural network consists of an input layer, two hidden-layers, respectively, and an output layer. First, the hidden layers apply linear transformations followed by Leaky ReLU functions [30]. The output layer implements again a linear transformation, and then a sigmoid function.

The qGAN is optimized with AMSGRAD [21] which is explicitly suitable for the implementation on real quantum hardware, since it is able to handle noisy gradients and non-stationary objective functions [20]. Furthermore, the training stability is improved by applying a gradient penalty on the discriminator [31, 32].

In each optimization epoch, the training data is shuffled and split into batches of size 1,000. The batches are used to update the parameters of the discriminator and the generator in an alternating fashion. After the updates are completed for all batches, a new epoch starts.

First, we present the results achieved when using a quantum simulator for the qGAN. The training involved 5,000 optimization epochs.

The training performance is illustrated in Fig. 3 with respect to the progress of the loss functions $L_D(\phi, \theta)$ and $L_G(\phi, \theta)$, the final cumulative distribution function (CDF) corresponding to $|g_\theta\rangle$, as well as the target CDF. The figures show that $|g_\theta\rangle$ truly converges towards the target distribution and that different initializations of the generator lead to different convergence behavior. In particular, the normal initialization outperforms the others.

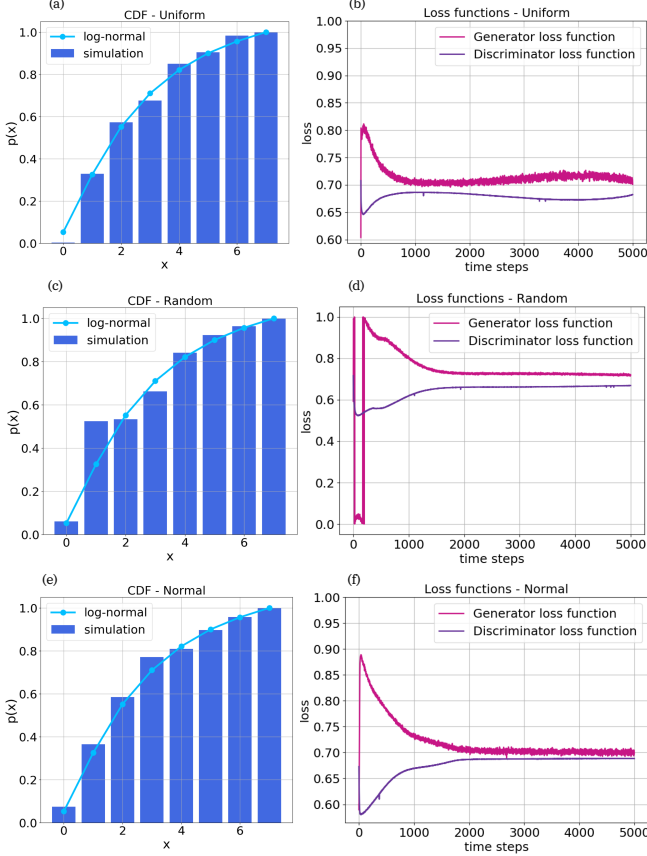


FIG. 3 Training the qGAN with a uniformly (a, b), a randomly (c, d), or a normally (e, f) initialized quantum generator gives the following results: The presented CDFs correspond to the trained $|g_\theta\rangle$ (a, c, e) and the training's progress is illustrated w.r.t. the loss functions (b, d, f).

Furthermore, we use the Kolmogorov-Smirnov statistic, see Appendix D, as a statistical measure to evaluate the qGAN performance. Given the null-hypothesis that the probability distribution from $|g_\theta\rangle$ is equivalent to the probability distribution underlying X , the Kolmogorov-Smirnov statistic D_{KS} determines whether the hypothesis is accepted or rejected with a certain confidence level, here set to 95%. The results presented in Table I confirm that using a normal initialization for the generator improves the outcome of the qGAN training.

The relative entropy is another measure that quantifies the difference between two probability distributions, see Appendix D for further details. Fig. 4 illustrates that the quantum generator continuously converges towards the training data's underlying distribution. As already

initialization	D_{KS}	Accept/Reject
uniform	0.098	Reject
random	0.245	Reject
normal	0.044	Accept

TABLE I Kolmogorov-Smirnov statistic for 500 randomly chose samples of $|g_\theta\rangle$ and the discretized, truncated log-normal distribution X .

observed before, the generator model which is initialized with a state that is already closer to the real distribution, i.e., the normally initialized generator, performs best.

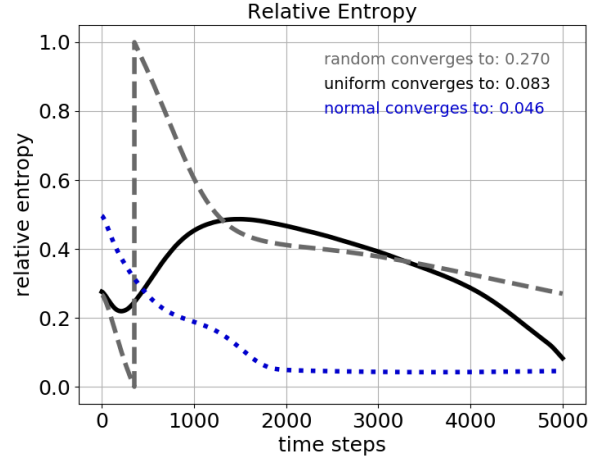


FIG. 4 This figure illustrates the convergence of the relative entropy for the period of 5,000 optimization steps for $|g_\theta\rangle$ with uniform/random/normal initialization.

Next, we present the results of the qGAN training run on an actual quantum processor, more precisely, the IBM Q 20 Poughkeepsie chip [18].

The same training data, quantum generator and discriminator as before are used. The initialization is chosen according to the normal setting because it achieved the best performance when running the training with a quantum simulation.

Out of all qubits on the chip, we chose 3 linearly connected qubits that have small error rates and run the training for 200 optimization epochs. The CDF corresponding to the resulting $|g_\theta\rangle$ and the progress of the loss functions are presented in Fig. 5.

As is known from classical GAN literature, it is not unusual that the loss functions do not clearly illustrate the method's convergence [33]. However, the progress of the relative entropy, see Fig. 6, shows a clear trend of $|g_\theta\rangle$ converging towards the random distribution underlying the training data samples.

Furthermore, it can be observed that the quantum hardware induces a certain level of noise. Although the noise impedes smooth convergence, it can also be helpful. More specifically, the noise induces fluctuations which can help to find good parameters at an early training

stage. As we can see in Fig. 6, the relative entropy in epoch 71 is particularly small, i.e. 0.055. Thus, we could run the training and, eventually, use the parameters that attained the smallest relative entropy.

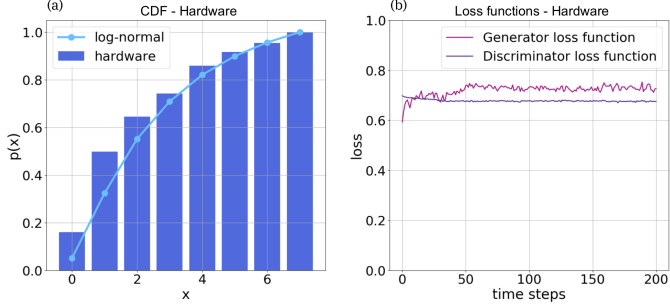


FIG. 5 The presented CDF (a) from $|g_\theta\rangle$ and the loss function progress (b) are achieved with a normally initialized qGAN training run on the IBM Q 20 Poughkeepsie.

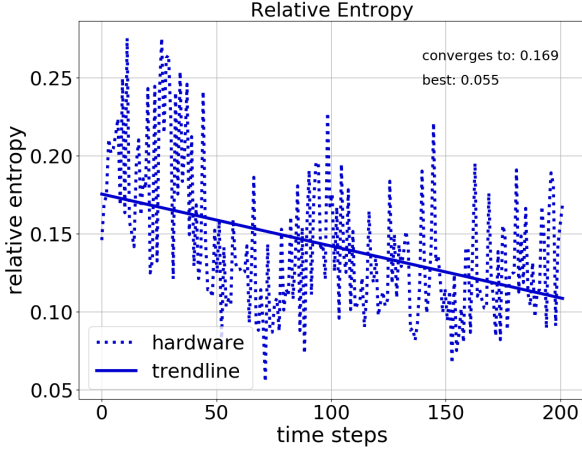


FIG. 6 Running the normally initialized qGAN with the IBM Q 20 Poughkeepsie chip gives the following results: (a) The presented CDF corresponds to the trained $|g_\theta\rangle$ (b) The training's progress is illustrated w.r.t. the loss functions.

Each epoch involves the execution of 1,000 quantum circuits to create the generated data batch, and then $12 \times 1,000$ circuits to compute the gradients for the update of the 6 parameters in θ . Given 200 optimization epochs, the total number of executed quantum circuits sums up to 2,600,000. Some of the more prominent fluctuations might be due to the fact that the IBM Q 20 Poughkeepsie chip is recalibrated on a daily basis which is, due to queuing, circuit preparation, and network communication overhead, shorter than the qGAN's training execution time.

B. European Option Pricing

In the following, the quantum channels trained with the qGANs are used to price European options. We compare the results from the best simulated quantum generator, i.e., the generator with a normal initialization, and the results from the generator run on real quantum hardware.

We use the trained quantum channels to load the learned random distribution describing the spot price at maturity S_T for a European call option. More specifically, we integrate the distribution loading quantum channel into a quantum algorithm based on QAE, see Appendix E, to evaluate the expected payoff $\max\{S_T - K, 0\}$ for $K = 2$, illustrated in Fig. 7. This algorithm achieves a quadratic speed-up compared to classically employed Monte Carlo methods if the data's underlying random distribution can be loaded efficiently. We refer to [22] for a detailed discussion of derivative pricing with QAE,

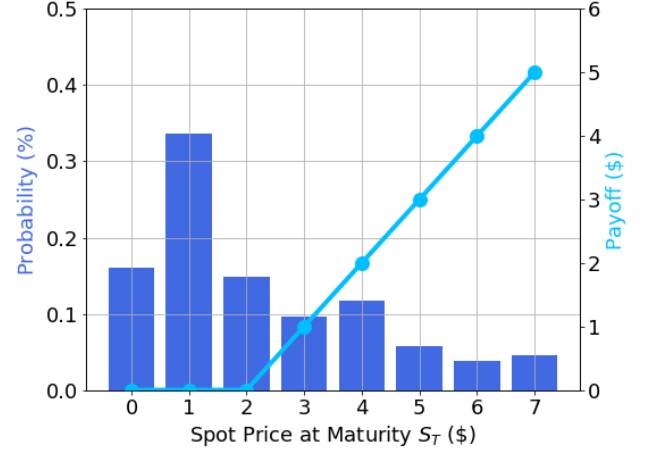


FIG. 7 Probability distribution of a spot price at maturity S_T and corresponding payoff function for a European Call option. The distribution has been learned with the qGAN described in IV A. Note that the model uses a normal initialization and is run on the IBM Q 20 Poughkeepsie chip.

The results for estimating $\mathbb{E}[\max\{S_T - K, 0\}]$ are given in Tab. II, where we compare

- an analytic evaluation with the exact truncated and discretized log-normal distribution p_{real} ,
- an analytic evaluation with the probability distribution given by $|g_\theta\rangle$ which was learned during the qGAN training run with quantum simulation,
- a QAE-based evaluation with the probability distribution given by $|g_\theta\rangle$ which was learned during the qGAN training run with quantum simulation,
- and a Monte Carlo (MC) simulation where the random samples are drawn by measuring $|g_\theta\rangle$ which

was learned during the qGAN training run on actual quantum hardware (IBM Q 20 Poughkeepsie).

The QAE-based approach uses $m = 5$ evaluation qubits, which implies the use of 32 quantum samples, and is run with a quantum simulation. It should be noted that improvements of the quantum hardware, i.e., longer decoherence times and better gate fidelities, are required to implement the QAE evaluation with actual quantum processors.

Moreover, we utilize the *true* randomness [34] of quantum measurements to run an MC simulation.

Approach	Distribution	Expected Payoff	#Samples
analytically	log-normal	1.0602	-
simulation	$ g_\theta\rangle$	0.9805	-
QAE + sim.	$ g_\theta\rangle$	1.2580	32
MC + real QC	$ g_\theta\rangle$	0.8836	8192

TABLE II Comparison of different approaches and models to evaluate $\mathbb{E}[\max\{S_T - K, 0\}]$.

The presented table illustrates that qGANs can be used to facilitate European call option pricing, potentially achieving quantum advantage.

V. CONCLUSION AND OUTLOOK

We demonstrated the application of an efficient probability distribution learning and loading scheme based on qGANs. The respective quantum channel is implemented by a gate-based quantum algorithm [3] and can, therefore, be directly integrated into other gate-based quantum algorithms. This is explicitly shown by the learning and loading a model for a European call option which is evaluated with a QAE-based algorithm that achieves a speed-up compared to classical Monte Carlo methods.

Current state-of-the-art techniques for loading generic random distributions into an n -qubit state necessitate $\mathcal{O}(2^n)$ gates [35]. Since this gate complexity can easily predominate a quantum algorithm's complexity, these techniques are not well suited for state initialization. Our distribution learning and loading scheme, on the other hand, only requires $\mathcal{O}(\text{poly}(n))$ many gates and can, therefore, be used for efficient state preparation.

Flexibility is given because the model can be fitted to the complexity of the underlying data and the loading scheme's resolution can be traded off against the complexity of the training data by varying the number of used qubits n and the circuit depth k .

Furthermore, the qGAN is compatible with online learning, i.e., the model can be updated if new training data samples become available. This can lead to a significant reduction of the training time in real-world learning scenarios.

However, some questions remain open and may be subject to future research. For example, an analysis of appropriate quantum circuit structures as well as optimal

training strategies remains open. Equivalent to classical machine learning, it is neither a-priori clear what model structure is the most suitable for a given problem nor what training strategy may achieve the best results.

Another interesting topic worth investigating considers the representation capabilities of qGANs with other data types. Encoding data into qubits' basis states naturally induces a discrete and equidistantly distributed set of represented data values. However, it might be interesting to investigate the compatibility of qGANs with continuous and non-equidistantly distributed values.

VI. ACKNOWLEDGMENTS

We would like to thank Giovanni Mariani for sharing his knowledge and engaging in very helpful discussions.

IBM and IBM Q are trademarks of International Business Machines Corporation, registered in many jurisdictions worldwide. Other product or service names may be trademarks or service marks of IBM or other companies.

Appendix A: Multivariate Historical Data for Portfolio Optimization

The qGAN scheme can also be used to learn and load multivariate random distributions. Here, we present the learning and loading of a distribution underlying the first two principle components of multivariate, constant maturity treasury rates of US government bonds. Note that the trained quantum channel can be used within the discussed QAE algorithm to evaluate, for instance, the fair price of a portfolio of government bonds, see [22].

The following results are computed with a quantum simulation. The training data set X consists of more than 5,000 samples, whereby data samples smaller than the 5%-percentile and bigger than the 95%-percentile have been discarded to reduce the number of required qubits for a reasonable representation of the distribution. The optimization scheme uses data batches of size 200 and is run for 20,000 training epochs.

Furthermore, we use a depth $k = 3$, unitary quantum generator that acts on $n = 6$ qubits, i.e., 3 qubits per dimension (principle component). The input state $|\psi_{\text{in}}\rangle$ is prepared as a multivariate uniform distribution and the generator parameters θ are initialized with random draws from a uniform distribution on the interval $[-\delta, +\delta]$ with $\delta = 10^{-2}$.

Here, the classical discriminator is composed of an input layer, two hidden-layers, respectively, and an output layer. Equivalently to the discriminator described in Sec. IV A, the hidden layers apply linear transformations followed by Leaky ReLU functions [30] and the output layer employs a linear transformation followed by a sigmoid function.

The convergence of the loss functions is illustrated in Fig. 8. The evolution of the relative entropy between the

generated and the real probability distribution is shown Fig. 9.

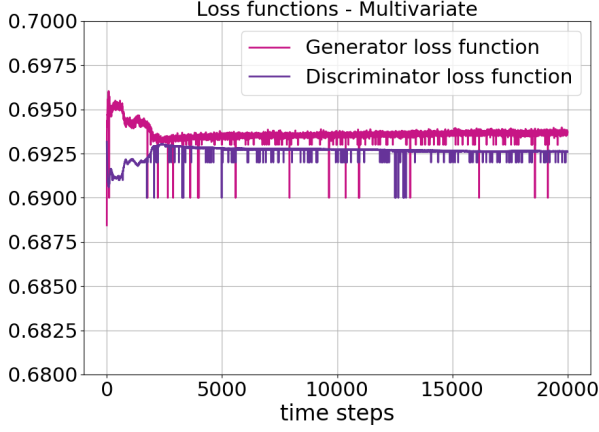


FIG. 8 Given historical multivariate government bond data, the progress of the generator's loss function and the discriminator loss function is shown for 20,000 optimization steps.

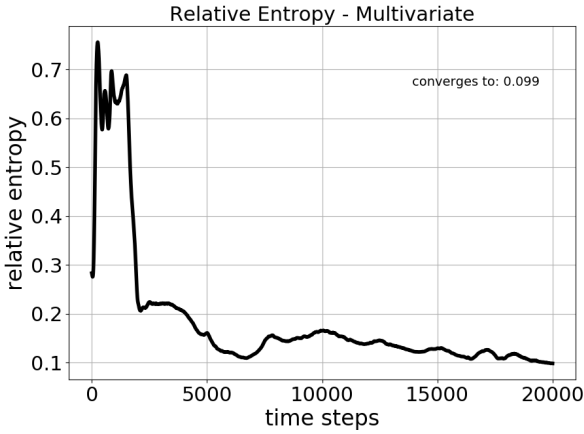


FIG. 9 This figure illustrates the convergence of the relative entropy between the quantum generator and the multivariate random distribution underlying the training data.

Appendix B: Isometric Quantum Generator

Closed quantum systems follow a unitary evolution. The unitary can be seen as an isolated black-box where the input state enters and a transformed state exits as output. The evolution of an open quantum system, i.e., a quantum system that interacts with an environment, evolves according to an isometry instead of a unitary [3].

In general, every isometry can be described by a unitary that acts on a larger system. In other words, an

isometry is given by a partial trace of a unitary quantum state evolution. The dynamics of an open quantum systems can be simulated by utilizing ancilla qubits. A quantum generator acting as an isometry can be implemented by using a minimum of one ancilla qubit. Depending on the setting, the use of an isometric quantum generator to learn random distributions, as described in Sec. IV A can be advantageous.

Appendix C: Analytic Gradients of a Variational Quantum Circuit

Compared to gradient-free optimization, gradient-based optimization methods have the potential to improve convergence rates, e.g. in a convex vicinity of local optima [36]. We now discuss a method to calculate analytic gradients [17, 37–40] for our variational circuit illustrated in Fig. 2.

The variational form used for the quantum generator applies parametrized single-qubit gates

$$R_Y(\theta) = e^{-i\frac{\theta}{2}Y} = \cos(\theta/2)I - i\sin(\theta/2)Y, \quad (C1)$$

where Y denotes the corresponding Pauli matrix [3] satisfying $Y^2 = I$ and $Y^\dagger = Y$. The respective derivative reads

$$\begin{aligned} \frac{\partial R_Y(\theta)}{\partial \theta} &= -\frac{i}{2}Y e^{-i\frac{\theta}{2}Y} \\ &= -\frac{1}{2}(i\cos(\theta/2)Y + \sin(\theta/2)I) \\ &= \frac{1}{2\sqrt{2}}(R_Y(\theta + \pi/2) - R_Y(\theta - \pi/2)). \end{aligned} \quad (C2)$$

Applying our n -qubit generator to the input state gives

$$\begin{aligned} |g_\theta\rangle &= G_\theta |\psi_{\text{in}}\rangle \\ &= \prod_{l=1}^k \left(\bigotimes_{i=1}^n (R_Y(\theta^{i,l})) U_{\text{ent}} \right) \bigotimes_{i=1}^n (R_Y(\theta^{i,0})) |\psi_{\text{in}}\rangle \\ &= \sum_{j=0}^{2^n-1} \sqrt{p_\theta^j} |j\rangle. \end{aligned} \quad (C3)$$

Recall that $|g_\theta\rangle$ is measured m times to obtain data samples g^l , $l \in \{1, \dots, m\}$ which can have 2^n different values. The generator loss function for a data batch of size m reads

$$L_G(\phi, \theta) = -\frac{1}{m} \sum_{l=1}^m [\log(D_\phi(g^l))], \quad (C4)$$

or equivalently,

$$L_G(\phi, \theta) = -\sum_{j=0}^{2^n-1} p_\theta^j \log(D_\phi(g^j)), \quad (C5)$$

with $p_\theta^j = \frac{\#j}{m}$, where $\#j$ denotes the number of times $|j\rangle$ is measured.

Updating the parameters θ with gradient based methods requires the evaluation of

$$\frac{\partial L_G(\phi, \theta)}{\partial \theta^{i,l}} = - \sum_{j=1}^m \frac{\partial p_\theta^j}{\partial \theta^{i,l}} \log(D_\phi(g^j)), \quad (C6)$$

whereby according to [39]

$$\frac{\partial p_\theta^j}{\partial \theta^{i,l}} = \frac{1}{2} \left(p_{\theta_+^{i,l}}^j - p_{\theta_-^{i,l}}^j \right). \quad (C7)$$

Here, $\theta_\pm^{i,l}$ is defined as $\theta \pm \frac{\pi}{2} e_{i,l}$ with $e_{i,l}$ denoting the (i, l) -unit vector of the respective parameter space.

Appendix D: Statistical Measures

Two different statistical measures are utilized to evaluate the performance of the qGAN. Both measures are defined as a distance of two (empirical) probability distributions P and Q .

The Kolmogorov-Smirnov statistic [41, 42] is based on the (empirical) cumulative distribution functions $P(X \leq x)$ and $Q(X \leq x)$ and is given by

$$D_{KS}(P||Q) = \sup_{x \in X} |P(X \leq x) - Q(X \leq x)|. \quad (D1)$$

The statistic can be used as a goodness-of-fit test. Given the null-hypothesis $P(x) = Q(x)$, we draw $s = 500$ samples from both distributions and choose a confidence level $(1 - \alpha)$ with $\alpha = 0.05$. The null-hypothesis is accepted if

$$D_{KS}(P||Q) \leq \sqrt{\frac{\ln \frac{2}{\alpha}}{s}} = 0.086. \quad (D2)$$

Another measure that can be used to characterize the closeness of (empirical) discrete probability distributions $P(x)$ and $Q(x)$ is the relative entropy, also called Kullback-Leibler divergence [3, 43]. This entropy-related measure is given by

$$D_{RE}(P||Q) = \sum_{x \in X} P(x) \log \left(\frac{P(x)}{Q(x)} \right). \quad (D3)$$

The relative entropy represents a non-negative quantity, i.e., $D_{RE}(P||Q) \geq 0$, where $D_{RE}(P||Q) = 0$ holds if $P(x) = Q(x)$, for all values x .

Appendix E: Quantum Amplitude Estimation

Given a quantum channel

$$\mathcal{A}|0\rangle^{\otimes n+1} = \sqrt{1-a}|\psi_0\rangle_n|0\rangle + \sqrt{a}|\psi_1\rangle_n|1\rangle, \quad (E1)$$

where $|\psi_0\rangle, |\psi_1\rangle$ denote n -qubit states, the QAE algorithm [4], illustrated in Fig. 10, enables the efficient evaluation of the amplitude a . The algorithm requires m additional evaluation qubits that control the applications of an operator $\mathcal{Q} = -\mathcal{A}\mathcal{S}_0\mathcal{A}^\dagger\mathcal{S}_{\psi_0}$ where $\mathcal{S}_0 = \mathbb{I}^{\otimes n+1} - |0\rangle\langle 0|^{\otimes n+1}$ and $\mathcal{S}_{\psi_0} = \mathbb{I}^{\otimes n+1} - |\psi_0\rangle\langle\psi_0| \otimes |0\rangle\langle 0|$. More precisely, evaluation qubit $j = 0, \dots, m-1$ controls operator \mathcal{Q}^{2^j} . Eventually, the error in the outcome scales with $\epsilon \propto \frac{1}{2^m}$, which corresponds to a quadratic speed-up compared to classical Monte Carlo simulation.

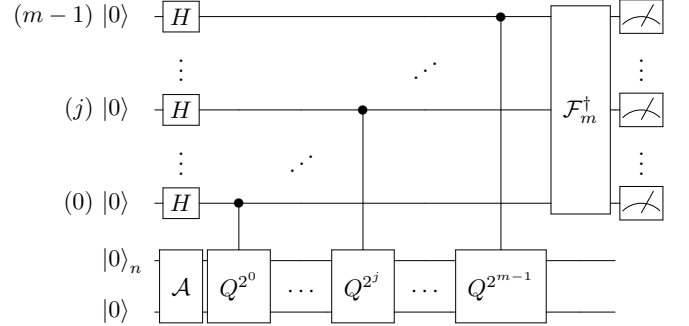


FIG. 10 The quantum circuit corresponding to Quantum Amplitude Estimation algorithm with the inverse Quantum Fourier Transform [3] being denoted by \mathcal{F}_m^\dagger .

To use QAE for the pricing of European options, we first need to load an uncertainty distribution into a quantum state, e.g., using qGANs, that represents the spot price S_T of the underlying asset at the option's maturity T . Suppose $|\psi\rangle_n = \sum_{i=0}^{2^n-1} \sqrt{p_i} |i\rangle_n$ corresponds to the loaded random distribution. Next, we add an ancilla qubit and use a comparator circuit that, depending on the strike price K , is given by

$$|i\rangle_n |0\rangle \mapsto \begin{cases} |i\rangle_n |0\rangle & , \text{ if } i \leq K \\ |i\rangle_n |1\rangle & , \text{ if } i > K. \end{cases} \quad (E2)$$

Last, we apply a function that maps the payoff to the amplitude of another ancilla qubit which is controlled by the previous comparison qubit. This results in the following quantum state

$$\sum_{i=0}^K \sqrt{p_i} |i\rangle_n |0\rangle |0\rangle + \sum_{i=K+1}^{2^n-1} \sqrt{p_i} |i\rangle_n |1\rangle \left(\sqrt{1-f(i)} |0\rangle + \sqrt{f(i)} |1\rangle \right), \quad (E3)$$

where we define $f(i) = \frac{i-K}{2^n-K-1}$. Thus, the probability of measuring $|1\rangle$ in the last qubit is equal to

$$\mathbb{P}[|1\rangle] = \frac{1}{2^n-K-1} \sum_{i=K+1}^{2^n-1} p_i (i-K) \quad (E4)$$

$$= \frac{1}{2^n-K-1} \mathbb{E}[\max\{0, S_T - K\}]. \quad (E5)$$

It follows that we can use QAE to approximate $\mathbb{P}[1]$, which, multiplied by $(2^n - K - 1)$, leads to an estimate for the expected payoff.

We apply the approximation scheme introduced in [22] and, therefore, avoid the involved implementation of the exact linear objective rotation given in Eq. (E3).

-
- [1] A. W. Harrow, A. Hassidim, and S. Lloyd, “Quantum algorithm for linear systems of equations,” *Physical Review Letters*, vol. 103, no. 15, pp. 1–8, 2009.
 - [2] S. Lloyd, M. Mohseni, and P. Rebentrost, “Quantum principal component analysis,” *Nature Physics*, vol. 10, 07 2013.
 - [3] M. A. Nielsen and I. L. Chuang, *Quantum Computation and Quantum Information*. Cambridge University Press, 2010.
 - [4] G. Brassard, P. Hoyer, M. Mosca, and A. Tapp, “Quantum Amplitude Amplification and Estimation,” *Contemporary Mathematics*, vol. 305, 2002.
 - [5] S. Aaronson, “Read the fine print,” *Nature Physics*, vol. 11, pp. 291–293, 2015.
 - [6] V. Giovannetti, S. Lloyd, and L. Maccone, “Quantum random access memory,” *Physical review letters*, vol. 100, p. 160501, 04 2008.
 - [7] W. K. Wootters and W. H. Zurek, “A single quantum cannot be cloned,” *Nature*, vol. 299, no. 5886, pp. 802–803, 1982.
 - [8] I. Goodfellow, J. Pouget-Abadie, M. Mirza, B. Xu, D. Warde-Farley, S. Ozair, A. Courville, and Y. Bengio, “Generative adversarial nets,” in *Advances in Neural Information Processing Systems 27*. Curran Associates, Inc., 2014, pp. 2672–2680.
 - [9] K. Kurach, M. Lucic, X. Zhai, M. Michalski, and S. Gelly, “The gan landscape: Losses, architectures, regularization, and normalization,” *CoRR*, vol. abs/1807.04720, 2018.
 - [10] S. Lloyd and C. Weedbrook, “Quantum generative adversarial learning,” *Phys. Rev. Lett.*, vol. 121, p. 040502, Jul 2018.
 - [11] M. Paris and J. Rehacek, *Quantum State Estimation*, 1st ed. Springer Publishing Company, Incorporated, 2010.
 - [12] P.-L. Dallaire-Demers and N. Killoran, “Quantum generative adversarial networks,” *CoRR*, vol. abs/1804.08641, 2018.
 - [13] M. Benedetti, E. Grant, L. Wossnig, and S. Severini, “Adversarial quantum circuit learning for pure state approximation,” 2018.
 - [14] L. Hu, S.-H. Wu, W. Cai, M. Yuwei, X. Mu, Y. Xu, H. Wang, Y. Song, D.-L. Deng, C.-L. Zou, and L. Sun, “Quantum generative adversarial learning in a superconducting quantum circuit,” *Science Advances*, vol. 5, 2019.
 - [15] H. Situ, Z. He, L. Li, and S. Zheng, “Quantum generative adversarial network for generating discrete data,” 2018.
 - [16] J. Romero and A. Aspuru-Guzik, “Variational quantum generators: Generative adversarial quantum machine learning for continuous distributions,” 2019.
 - [17] J. Zeng, Y. Wu, J.-G. Liu, L. Wang, and J. Hu, “Learning and inference on generative adversarial quantum circuits,” *CoRR*, vol. abs/1808.03425, 2018.
 - [18] “IBM Q Experience.” [Online]. Available: <https://quantumexperience.ng.bluemix.net/qx/experience>
 - [19] W. Fedus, M. Rosca, B. Lakshminarayanan, A. M. Dai, S. Mohamed, and I. Goodfellow, “Many paths to equilibrium: GANs do not need to decrease a divergence at every step,” in *International Conference on Learning Representations*, 2018.
 - [20] D. P. Kingma and J. Ba, “Adam: A method for stochastic optimization,” *CoRR*, vol. abs/1412.6980, 2014.
 - [21] S. J. Reddi, S. Kale, and S. Kumar, “On the convergence of adam and beyond,” in *International Conference on Learning Representations*, 2018.
 - [22] S. Woerner and D. J. Egger, “Quantum risk analysis,” *npj Quantum Information*, vol. 5, 12 2019.
 - [23] J. McClean, S. Boixo, V. N. Smelyanskiy, R. Babbush, and H. Neven, “Barren plateaus in quantum neural network training landscapes,” *Nature Communications*, vol. 9, 03 2018.
 - [24] L. Grover and T. Rudolph, “Creating superpositions that correspond to efficiently integrable probability distributions,” 2002.
 - [25] J. McClean, J. Romero, R. Babbush, and A. Aspuru-Guzik, “The theory of variational hybrid quantum-classical algorithms,” *New Journal of Physics*, vol. 18, 09 2015.
 - [26] I. Goodfellow, Y. Bengio, and A. Courville, *Deep Learning*. MIT Press, 2016.
 - [27] F. Black and M. Scholes, “The pricing of options and corporate liabilities,” *Journal of Political Economy*, vol. 81, no. 3, pp. 637–654, 1973.
 - [28] G. Aleksandrowicz, T. Alexander, P. Barkoutsos, L. Bello, Y. Ben-Haim, D. Bucher, F. J. Cabrera-Hernández, J. Carballo-Franquis, A. Chen, C.-F. Chen, J. M. Chow, A. D. Córcoles-Gonzales, A. J. Cross, A. Cross, J. Cruz-Benito, C. Culver, S. D. L. P. González, E. D. L. Torre, D. Ding, E. Dumitrescu, I. Duran, P. Eendebak, M. Everitt, I. F. Sertage, A. Frisch, A. Fuhrer, J. Gambetta, B. G. Gago, J. Gomez-Mosquera, D. Greenberg, I. Hamamura, V. Havlicek, J. Hellmers, L. Herok, H. Horii, S. Hu, T. Imamichi, T. Itoko, A. Javadi-Abhari, N. Kanazawa, A. Karazeev, K. Krsulich, P. Liu, Y. Luh, Y. Maeng, M. Marques, F. J. Martín-Fernández, D. T. McClure, D. McKay, S. Meesala, A. Mezzacapo, N. Moll, D. M. Rodríguez, G. Nannicini, P. Nation, P. Ollitrault, L. J. O’Riordan, H. Paik, J. Pérez, A. Phan, M. Pistoia, V. Prutyanov, M. Reuter, J. Rice, A. R. Davila, R. H. P. Rudy, M. Ryu, N. Sathaye, C. Schnabel, E. Schoute, K. Setia, Y. Shi, A. Silva, Y. Siraichik, S. Sivarajah, J. A. Smolin, M. Soeken, H. Takahashi, I. Tavernelli, C. Taylor, P. Taylour, K. Trabing, M. Treinish, W. Turner, D. Vogt-Lee, C. Vuillot, J. A. Wildstrom, J. Wilson, E. Winston, C. Wood, S. Wood, S. Woerner, I. Y. Akhalwaya, and C. Zoufal, “Qiskit: An open-source framework for quantum computing,” 2019.
 - [29] “Pytorch.” [Online]. Available: <https://pytorch.org>
 - [30] D. Pedamonti, “Comparison of non-linear activation functions for deep neural networks on mnist classification task,” *CoRR*, vol. abs/1804.02763, 2018.
 - [31] N. Kodali, J. D. Abernethy, J. Hays, and Z. Kira, “On

- convergence and stability of gans,” 2017.
- [32] K. Roth, A. Lucchi, S. Nowozin, and T. Hofmann, “Stabilizing training of generative adversarial networks through regularization,” in *NIPS*, 2017.
 - [33] P. Grnarova, K. Y. Levy, A. Lucchi, N. Perraudin, T. Hofmann, and A. Krause, “Evaluating gans via duality,” *CoRR*, vol. abs/1811.05512, 2018.
 - [34] S. Pironio, “The certainty of quantum randomness,” *Nature*, vol. 556, pp. 176–177, 04 2018.
 - [35] M. Plesch and Č. Brukner, “Quantum-state preparation with universal gate decompositions,” *Phys. Rev. A*, vol. 83, 03 2010.
 - [36] A. Harrow and J. Napp, “Low-depth gradient measurements can improve convergence in variational hybrid quantum-classical algorithms,” 01 2019.
 - [37] E. Farhi and H. Neven, “Classification with quantum neural networks on near term processors,” 02 2018.
 - [38] M. Schuld, A. Bocharov, K. M. Svore, and N. Wiebe, “Circuit-centric quantum classifiers,” 2018.
 - [39] K. Mitarai, M. Negoro, M. Kitagawa, and K. Fujii, “Quantum circuit learning,” *Phys. Rev. A*, vol. 98, p. 032309, Sep 2018.
 - [40] J.-G. Liu and L. Wang, “Differentiable learning of quantum circuit born machines,” *Phys. Rev. A*, vol. 98, p. 062324, Dec 2018.
 - [41] I. Chakravarti, R. Laha, and J. Roy, *Handbook of methods of applied statistics*, ser. Wiley series in probability and mathematical statistics. Wiley, 1967, no. Vol. 1.
 - [42] A. Justel, D. Peña, and R. Zamar, “A multivariate kolmogorov-smirnov test of goodness of fit,” *Statistics and Probability Letters*, vol. 35, no. 3, pp. 251 – 259, 1997.
 - [43] S. Kullback and R. A. Leibler, “On information and sufficiency,” *Ann. Math. Statist.*, vol. 22, no. 1, pp. 79–86, 03 1951.